In vivo coating of bacterial magnetic nanoparticles by magnetosome expression of spider silk-inspired peptides

*Frank Mickoleit[1], Christian B. Borkner[2], Mauricio Toro-Nahuelpan[1,3], Heike M. Herold[2], Denis S. Maier[1], Jürgen M. Plitzko[3], Thomas Scheibel[2,4,5,6,7,8] & Dirk Schüler[1]**

[1]Dept. Microbiology / [2]Dept. Biomaterials / [4]Bayerisches Polymerinstitut (BPI) / [5]Bayreuther Zentrum für Kolloide und Grenzflächen (BZKG) / [6]Institut für Bio-Makromoleküle (bio-mac) / [7]Bayreuther Zentrum für Molekulare Biowissenschaften (BZMB) / [8]Bayreuther Materialzentrum (BayMAT), University of Bayreuth, D-95447 Bayreuth, Germany; [3]Dept. Molecular Structural Biology, Max Planck Institute of Biochemistry, D-82152 Martinsried, Germany

KEYWORDS. *Magnetosprillum gryphiswaldense*; magnetosomes; surface functionalization; spider silk; biocomposite; hybrid proteins

ABSTRACT. Magnetosomes are natural magnetic nanoparticles with exceptional properties that are synthesized in magnetotactic bacteria by a highly regulated biomineralization process. Their usability in many applications could be further improved by encapsulation in biocompatible polymers. In this study, we explored the production of spider silk-inspired peptides on magnetosomes of the alphaproteobacterium *Magnetospirillum gryphiswaldense*. Genetic fusion of different silk sequence-like variants to abundant magnetosome membrane proteins enhanced magnetite biomineralization and caused the formation of a proteinaceous capsule, which increased the colloidal stability of isolated particles. Furthermore, we show that spider silk peptides fused to a magnetosome membrane protein can be used as seeds for silk fibril growth on the magnetosome surface. In summary, we demonstrate that the combination of two different biogenic materials generates a genetically encoded hybrid composite with engineerable new properties and enhanced potential for various applications.

Introduction

Magnetosomes are membrane-enveloped magnetic nanoparticles (MNPs) biomineralized by magnetotactic bacteria, in which they serve as geomagnetic field sensors.[1,2] In the alphaproteobacterium *Magnetospirillum gryphiswaldense* they are composed of a monocrystalline magnetite (Fe_3O_4) core enveloped by the magnetosome membrane, which consists of phospholipids and a set of specific proteins.[3] Due to their highly regulated biosynthesis, magnetosomes exhibit unprecedented characteristics such as high crystallinity, strong magnetization, as well as uniform shapes and sizes.[4,5] These features make them ideal for numerous biomedical and biotechnological applications, for instance magnetic capturing of

soluble analytes,[6] magnetosome-based immunoassays,[7] as nanocarriers for magnetic drug targeting,[8] magnetic hyperthermia,[9,10] and as reporters for magnetic resonance imaging (MRI)[11,12] and magnetic particle imaging (MPI).[13] For many of these applications magnetosomes have to be further functionalized by the introduction of additional moieties to the surface, or by encapsulation of the particles, especially if they are intended for the use as theranostics. As one of the most attractive features of magnetosomes both their crystal morphologies and the composition of the enveloping membrane can be engineered *in vivo* by genetic means. Abundant magnetosome membrane (Mam) proteins can be used as fusion anchors for surface display of foreign proteins and peptides. For example, both the N- and C-terminus of the 12.4-kDa MamC protein that has only a minor function in magnetite biomineralization[14-16] provide sites for covalent and highly specific attachment of foreign proteins to the magnetosome surface by genetic fusion.[17-19] MamC has been used for the magnetosome expression of the fluorophore (e)GFP,[17,18] camelid antibody fragments (nanobodies),[6,20] and enzymes such as luciferase,[21] the multi-subunit chimeric bacterial RNase P[22] or the paraoxonase Opd.[23] Using an improved expression system[18] and a recombination-impaired bacterial strain,[24] even arrays of up to five copies of the enzyme glucuronidase (GusA) fused to a terminal, codon-optimized eGFP (mEGFP) as additional reporter could be expressed on the magnetosome surface.[25] In the latter study, MamC, GusA monomers and mEGFP were stitched together by flexible Gly_{10} linkers, which are known to allow proper folding of recombinant proteins and thus, ensure biological activity.[26] In addition, Borg and co-workers generated hybrid core-shell nanoparticles, consisting of the fluorescent magnetosome core (expressing eGFP) enclosed by a ZnO or silica shell,[27] which improved colloidal stability.

A further intriguing material suitable for coatings could be spider silk, which exhibits extraordinary properties such as a high toughness combined with good biocompatibility[28-30] desirable for future *in vivo* applications of bacterial magnetosomes. Spider silk proteins (so-called spidroins) consist of non-repetitive terminal domains that flank the highly repetitive core domain and often exceed a molecular weight of 150 kDa.[29] However, recombinant expression of spider silk proteins in bacteria so far has been confined to only few well-established systems such as *Escherichia coli*, *Salmonella* and *Bacillus* sp. species.[31-33]

In this study, we explored the expression of spider silk sequences on the magnetosome surface of the magnetotactic alphaproteobacterium *M. gryphiswaldense*. The recombinant engineered spider silk protein eADF4 (engineered *Araneus diadematus* fibroin 4) is based on the consensus sequence of the highly repetitive primary structure of ADF4,[34,35] and the number of repeat units can be adjusted allowing the production of spidroins with various molecular weights.[36] The engineered consensus sequence is called module C consisting of 35 amino acids (GSSAAAAAAAASGPGGYGPENQGPSGPGGYGPGGP).[35,37,38] We show that silk motifs (based on module C) can be conjugated to a single MamC anchor by genetic fusion. Silk expression enhanced magnetosome biosynthesis and caused the formation of a proteinaceous capsule, which increased the colloidal stability of isolated particles. Overall, this demonstrates that two different biogenic materials, spider silk and magnetosomes, can be genetically combined, thereby generating a new hybrid composite with novel properties and enhanced application potential.

Materials and Methods

Bacterial strains, plasmids, and cultivation conditions

Bacterial strains and plasmids that were used in this study are listed in Tables S1 and S2, respectively. *M. gryphiswaldense* strains were grown microaerobically in modified flask standard medium (FSM) at 30°C according to *Heyen and Schüler*.[39] Magnetite formation was ensured by applying a headspace-to-liquid ratio of approximately 1:4 with air in the headspace. Oxygen concentrations declined from high initial levels in the medium with increasing cell numbers, eventually reaching low dissolved oxygen concentrations, permitting magnetite synthesis.[17] *E. coli* strains were grown as previously described.[40] For the cultivation of *E. coli* WM3064 D,L-α,ε-diaminopimelic acid (DAP) was added to lysogeny broth (LB) medium at a final concentration of 1 mM. Strains were routinely cultured as previously described.[18] For the cultivation on solid medium 1.5% (w/v) agar was added. For strains carrying recombinant plasmids, media were supplemented with 25 µg/ml kanamycin (Km) for *E. coli* and 5 µg/ml for *M. gryphiswaldense* strains.

Molecular and genetic techniques

Oligonucleotides (see Table S3) were purchased from Sigma-Aldrich (Steinheim, Germany). Plasmids were constructed by standard recombinant techniques as described in detail below. All constructs were sequenced by Macrogen Europe (Amsterdam, Netherlands). Sequence data were analyzed with Geneious 8.0.5 (Biomatters Ltd) and ApE 2.0.47 (M. Wayne Davis, 2009).

Construction of MamC fusion proteins

The *c2* sequence was amplified from pCS-eADF4(C2) using the primers linker1-sps fwd and sps rev. The resulting fragment was subsequently inserted into the NcoI and BamHI restriction sites of pSB9, thereby generating pFM-C2. For construction of pFM1 and pFM2, first the *cl2* and *cl32* sequences were generated via several PCR steps (Figure S1 - S3). The primer combinations linker1-sps fwd and sps-linker2 rev, or linker2-sps fwd and sps rev were used to amplify the *c*-module, with pCS-eADF4(C16) serving as template. Due to the repetitive *c16* sequence, in both reactions fragments of different sizes (ranging from 105 to 10,500 bp) were obtained. The *c1* fragments (105 bp) were chosen and fused via overlap PCR, resulting in the 276 bp sequence *gly10-c1-gly10-c1*, referred to as *cl2*. After restriction with NcoI and BamHI, *cl2* was cloned into pSB9, thereby replacing *gusA* and generating pFM1. For the construction of *cl32*, the *cl2* sequence was amplified using primer combinations linker1-sps fwd / sps-linker3 rev or linker3-sps fwd / sps-linker4 rev. The resulting fragments were subjected to overlap PCR as described above, thereby generating a *cl4* fragment. The *cl32* sequence $(gly10\text{-}c1)_{32}$ was obtained by overlap PCR using *cl4* as template. Due to the repetitive *cl4* structure, *cl6*, *cl8*, *cl16* and *cl32* sequences were obtained. *cl32* was chosen and amplified using the primers linker1-sps fwd and sps rev to generate NcoI and BamHI restriction sites. After digestion, *cl32* was cloned into pSB9, thereby replacing *gusA* and generating pFM2.

pFM-C2, pFM1 or pFM2 were transferred to *M. gryphiswaldense* strains by conjugation, with the expression cassettes being chromosomally inserted by Tn5 transposition.

Determination of iron

Iron content of cells and isolated magnetosomes were determined by flame atomic absorption spectroscopy. Magnetosomes or cells (suspensions with equal optical densities) were pelleted, resuspended in 0.5 ml 69% nitric acid and incubated at 98°C for 3 h. The measurements were conducted with a Perkin-Elmer Atomic Absorption Spectrometer 1100 B (Überlingen, Germany) using the following conditions: wavelength 248 nm, gap width 0.2 nm, lamp current 20 mA.

UV/Vis spectroscopy

Optical density (OD) and magnetic response (C_{mag}) of late exponentially phase cells were measured photometrically at 565 nm as previously reported.[41] Briefly, for C_{mag} measurements, cells were aligned parallel to the field lines of a magnetic field, resulting in a change in light scattering. The ratio of scattering intensities at different field angles relative to the light beam was used to characterize the average magnetic orientation of the cells. C_{mag} is well correlated to the average number of magnetosomes in magnetic cell populations and, thus, can be used for semi-quantitative estimations of magnetosome contents.

Transmission electron microscopy

For TEM of whole cells and isolated magnetosomes, specimens were directly deposited onto carbon-coated copper grids. Magnetosomes were stained with 1% uranyl acetate. Transmission electron microscopy was performed on a CEM 902A (Zeiss, Oberkochen, Germany) with an acceleration voltage of 80 kV. Images were taken with a Gata Erlangshen ES500W CCD camera. Sizes of crystals were measured with ImageJ software.

Analysis of sedimentation behavior / colloidal stability

Sedimentation analyses of isolated magnetosomes were performed as previously described.[42,43] Nanoparticle dispersions were fractioned by gravity and allowed to settle for 60 min. During this incubation time agglomerates (e.g. particles that have accidently lost their membrane) formed pellets at the bottom of the tube. The supernatants were collected and subjected to the sedimentation assay. Assuming that the dispersions contained particles with equal size distributions (at the beginning of the experiment), the sedimentation rates depended only on the aggregation process. Sedimentation profiles were obtained by measuring the optical density as a function of time at a wavelength of 508 nm. Absorption values were normalized with the absorption at the initial time of the experiment, thus allowing direct comparisons of the different dispersions.

Zetasizer measurements

Zeta potential (ZP) values and particle sizes were determined with a Zetasizer Nano (Malvern, UK). Suspensions of isolated magnetosomes (wild type or spider silk decorated particles) were pelleted and resuspended in 10 mM Hepes + 1 mM EDTA buffer, pH 7.2. For ZP measurements DTS1070 folded capillary cells (Malvern, UK) were used. Measurements were made in triplicates.

Biochemical methods

Isolation of bacterial magnetosomes from *M. gryphiswaldense* was performed as previously described.[17,39] Denaturing polyacrylamide gels were prepared according to the method of *Laemmli*,[44] modified after *Fling and Gregerson*.[45] Samples of isolated magnetosomes contained

32 µg Fe, and the solubilized magnetosome membrane proteins were separated by electrophoresis and subsequently transferred onto polyvinylidene difluoride (PVDF) membranes (Roth, Germany). For immunological detection, membranes were blocked / equilibrated in AP-T buffer (0.1 M Tris; 0.1 M NaCl; 5 mM $MgCl_2$ x 6 H_2O; 0.05% (v/v) Tween 20; pH 7.4) for 2 h. Primary rabbit anti-MamC IgG antibody was added at a 1 : 3,000 ratio and incubated for 2 h at room temperature. Membranes were subsequently washed 4-times with AP-T buffer for 5 min and incubated with a secondary goat anti-rabbit IgG antibody (1:30,000; anti-rabbit IgG with conjugated alkaline phosphatase [Sigma Aldrich, Steinheim, Germany]) for 1 h. Membranes were again washed 4-times with AP-T buffer for 5 min, and finally 15 min in AP buffer (0.1 M Tris; 0.1 M NaCl; 5 mM $MgCl_2$; pH 9.5). For staining / detection, the membrane was transferred to a BCIP / NBT substrate solution and incubated until violet bands appeared. The reaction was stopped with acidified water.

Cryo-electron tomography (CET)

Plunge-freezing vitrification: 5 µl of MSR culture mixed with 2 µl of 15 nm BSA-coated colloidal gold clusters (Sigma Aldrich, Steinheim, Germany) was used for subsequent alignment purposes. The mixture was added on glow-discharged Quantifoil R 2/1 holey carbon molybdenum grids (Quantifoil Micro Tools GmbH, Jena, Germany), blotted and embedded in vitreous ice by plunge freezing into liquid ethane (< −170°C). The grids were stored in sealed boxes in liquid nitrogen until used.

CET: Tomography was performed under low-dose conditions using a Tecnai G2 Polara transmission electron microscope (FEI) equipped with a 300 kV field emission gun, and a Gatan GIF 2002 post-column energy filter. A 3838 x 3710 Gatan K2 Summit Direct Detection Camera

operated in counting and dose-fractionation mode was used for imaging. Data collection was performed at 300 kV, with the energy filter operated in the zero-loss mode (slit width of 20 eV). Tilt series were acquired using Serial EM software.[46] The specimen was tilted about one axis with 1.5° increments over a typical total angular range of ± 60°. The cumulative electron dose during the tilt series was kept below 150 e^{-} $Å^{-2}$. To account for the increased specimen thickness at high tilt angles, the exposure time was multiplied by a factor of 1/cos α. Pixel size at the specimen level was 4.27 Å at an EFTEM magnification of 27500x. Images were recorded at nominal −6 μm defocus.

Tomogram reconstruction and segmentation: Tomograms were reconstructed in the IMOD package.[47] Tomographic reconstructions from tilt series were performed with the weighted back-projection with IMOD software using particles as a fiducial marker. Aligned images were binned to the final pixel size of 17.08 Å for WT (9 tomograms), *mamC-cl2* (8 tomograms) and *mamC-cl32* (11 tomograms) non-magnetic cells treated under low iron conditions and 25.62 Å for the *mamC-cl32* strain grown in FSM media (10 tomograms from 10 cells). For tomographic reconstruction, the radial filter options were cut off: 0.5 and fall off: 0.05. The dataset for this study consisted of 38 tomograms from 38 cells. Tomograms were treated with an anisotropic nonlinear diffusion denoising algorithms to improve signal-to-noise ratio.

Segmentation of the tomogram was done with Amira software on binned volumes of magnetic cells of the *mamC-cl32* strain with a voxel size of 25.62 Å. Membrane segmentation was done using the software TomoSegMemTV and a complementary package, SynapSegTools, both for Matlab.[48] Tomograms visualization and membrane thickness measurements were performed in 3dmod software from the IMOD package.

Attenuated total reflection fourier transform infrared spectroscopy (ATR-FTIR)

Magnetosome samples were dispersed in water at a concentration of 1.5 mg/ml, and 2 µl magnetosome dispersion were placed on the Ge crystal. The samples were dried and ATR-FTIR spectra were measured on a Ge crystal using a MIRacle^{TM} Single Reflection ATR accessory (PIKE Technologies, Madison, USA) with a Bruker Tensor 27 spectrometer (Bruker, Germany) between 4000 cm^{-1} and 800 cm^{-1}. Each measurement reflects 120 scans at a resolution of 2 cm^{-1}. Spectra are focused between 1770 cm^{-1} and 1580 cm^{-1} to highlight relevant and significant differences in the absorbance region of C=O stretching vibrations of lipids and proteins. A baseline correction was applied using OPUS software (Bruker Optics Corp., USA) and spectra were normalized (A/A_{max}). The relation of the absorption maxima of the phospholipid/lipid band (~ 1750 cm^{-1} – 1710 cm^{-1}) and amide I band of proteins (~ 1690 cm^{-1} – 1600 cm^{-1}) was calculated by $A_{norm.}$(amide I)/$A_{norm.}$(phospholipids).

Quartz crystal microbalance with dissipation monitoring (QCM-D)

Sensor chip coating with eADF4(C16): QCM-D resonators (5 MHz, AT-cut, Cr/Au; Quartz Pro Sweden AB, Järfälla, Sweden) were cleaned by a 10 min UV/ozone treatment (PSD-Pro Series, Novascan, Ames, USA) followed by spin coating (4000 rpm, 1800 rpm/s, 30s; 1-EC 101 DT 8-19456 Spin-Coater, Headway Research Inc., Garland, USA) with 30 µl eADF4(C16) (AMSilk GmbH, Planegg/München, Germany) solution (1 mg/ml) in formic acid (Sigma-Aldrich, Steinheim, Germany). The eADF4(C16)-coated sensor chips were post treated in methanol atmosphere overnight, and mounted in the standard Q-Sense flow module (QFM 401, Biolin Scientific, Västra Frölunda, Sweden).

Magnetosome adsorption study: All equilibration and adsorption steps were performed in Hepes buffer (10 mM Hepes, 1 mM EDTA, pH 7.2) at a volume flow of 70 ml/min at 21°C with a Q-Sense E4 (Biolin Scientific, Västra Frölunda, Sweden). The coated sensor chips (eADF4(C16)) were equilibrated in buffer, flushed with 100 µg/ml magnetosomes (wild type and *mamC-c2*) for 40 min followed by a 50 min buffer flow again. Frequency and dissipation data are monitored for the 3rd overtone. The change in areal mass density $\Delta\rho_A$ for a specific overtone n is proportional to the change in frequency Δf and described by Sauerbrey equation (Eq. 1).[49]

$$\Delta\rho_A = -\frac{\rho_q h_q}{f_0}\frac{\Delta f}{n} = -C\frac{\Delta f}{n} \qquad (1)$$

The mass sensitivity constant C depends on the density (ρ_q), the thickness (h_q) and the fundamental frequency (f_0) of the quartz crystal.[50]

Fibrillization experiments

eADF4(C16) protein was produced as published previously.[34] Aqueous eADF4(C16) solutions were prepared by dissolving lyophilized protein in 6 M guanidinium thiocyanate (GdmSCN) followed by dialysis against 10 mM Tris/HCl, pH 7.5, with three buffer changes, twice after 2 h and once after 16 h. The protein concentration was determined using a Varian Cary 50 Bio UV–Vis spectrometer after centrifugation in a Beckman Optima ultracentrifuge at 55,000 rpm for 45 min at 20°C. Isolated MamC-C2 or wild type magnetosomes (0.5 mg/ml Fe) were used as seeds in fibrillization experiments and added to an eADF4(C16) solution (1 mg/ml) in the presence of 100 mM potassium phosphate (pH 7.4).

Results and Discussion

Construction of spider silk motif expressing *M. gryphiswaldense* strains

An engineered version of *adf4* (codon-optimized for recombinant expression in *E. coli*)[34,35,51] was used as template for the generation of repetitive spider silk sequences. By designing engineered spider silk motifs for expression on magnetosomes, two strategies were explored: (i) Glycine linkers could improve folding of recombinant fusion proteins and also reduce sterical hindrance,[26] and therefore spider silk-like constructs containing Gly_{10} linkers were designed. Single C motifs were connected by Gly_{10} and the resulting arrays with two or 32 silk units (referred to as CL2 or CL32, respectively) were genetically fused to the magnetosome membrane protein MamC. On the other hand, previous computational analysis and *in vitro* measurements have shown that the structural properties of silks (like their unique pattern of extreme solubility inside the spider glands and complete insolubility outside) depend on their highly repetitive, uninterrupted hydrophobic regions and that their characteristics might be affected by very small changes in the protein sequence.[52] We (ii) also generated a construct with the established C2 peptide[36] connected to MamC. Translational fusions of *c2* or *cl2* / *32* to *mamC* were designed as *mamC-c2* or *mamC-cl2* / *32* constructs (Figure 1) under control of the constitutive, optimized $P_{mamDC45}$ promotor and the optimized ribosome binding site (oRBS), which allow high-level expression of foreign proteins.[18] *mamC-c2* or *mamC-cl2* / *32* cassettes were inserted via Tn5 transposition at random chromosomal positions and expressed in RecA-deficient strain *M. gryphiswaldense* IK-1 to avoid homologous recombination between identical sequences.[24]

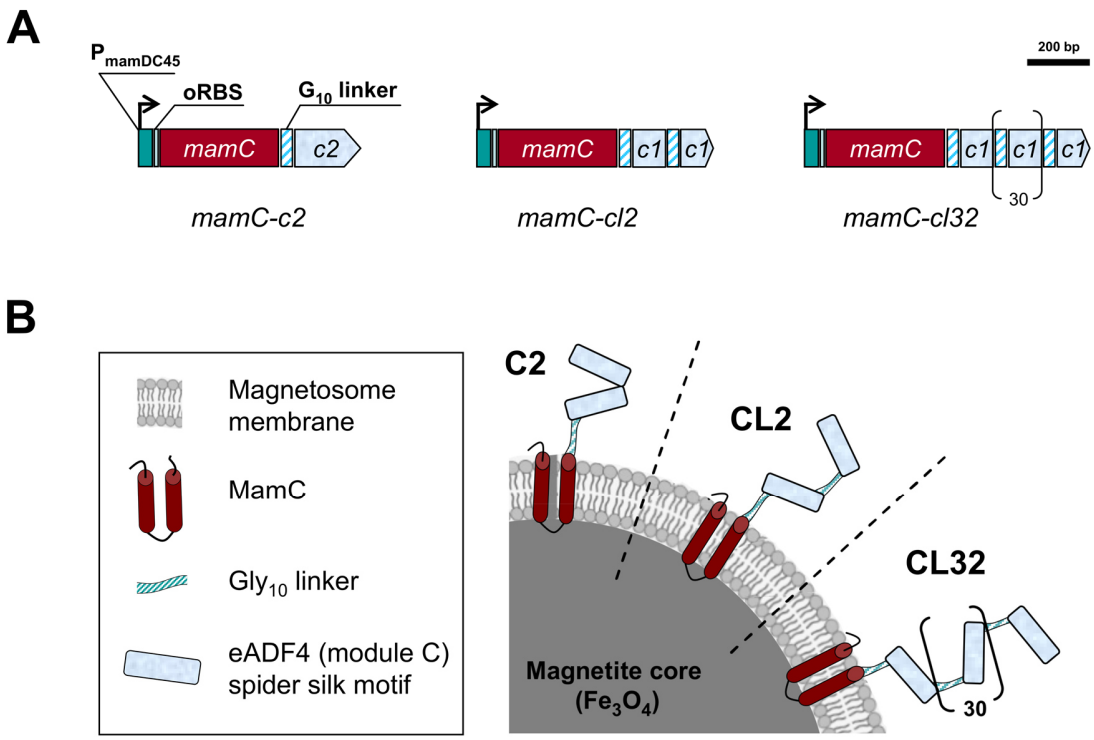

Figure 1. (A) Schematic representation showing the genetic organization of the expression cassettes for magnetosome display of spider silk motifs (MamC-C2, MamC-CL2 and MamC-CL32). (B) Schematic of spider silk motifs C2, CL2 and CL32 produced as hybrid-proteins fused to a single MamC membrane anchor. For more details, refer to the methods section (size of particle and proteins not to scale).

Expression of linker-modified, silk-like constructs in *M. gryphiswaldense* impairs cell division and increases magnetosome biomineralization

M. gryphiswaldense strains *mamC-c2* and *mamC-cl2 / 32* grew slightly slower compared to the parental strain IK-1 (doubling times: *mamC-c2*, 6.1 h; *mamC-cl2*, 6.2 h; *mamC-cl32*, 6.5 h; IK-1, 5.9 h). The magnetic response (C_{mag}) of *mamC-c2* cells was comparable to that of IK-1 (*mamC-*

c2: 0.91 ± 0.07; IK-1: 0.94 ± 0.05); however, for strains *mamC-cl2* and *mamC-cl32*, C_{mag} values decreased with the number of spider silk motifs (*mamC-cl2*: 0.83 ± 0.02; *mamC-cl32*: 0.64 ± 0.09). Iron contents and total particle numbers per cell were increased for *mamC-cl2* and *mamC-cl32* by 66% and 71%, respectively, with up to 60 magnetosomes per cell on average. One can speculate that the observed reduced growth rates favor an increased magnetosome production. Nearly 40% of the cells (*mamC-cl2*: 36.2%; *mamC-cl32*: 38.3%) contained less than 20 particles, whereas more than 50% (*mamC-cl2*: 51.7%; *mamC-cl32*: 53.0%) contained more than 80 particles (*mamC-cl2*: 97 ± 14; *mamC-cl32*: 104 ± 13) partially resembling overproducer strains engineered before.[53] Only a low number of cells (6%) produced wild type-like particle amounts (Figure 2 and Figure S5). In contrast, strain *mamC-c2* showed a wild type-like particle number distribution and synthesized wild type-like amounts of magnetosomes (32 ± 11 particles per cell; Figure 2 and Figure S4) arranged in one or two chains positioned ad midcell.

The spatial stochastic resonance in the sequence hydrophobicities of spider silk proteins[52,54] is highly sequence dependent. Even small changes in the spider silk protein sequence, like the Gly_{10} linker introduction into constructs MamC-CL2 and MamC-CL32, might affect these resonance properties, which could be experimentally confirmed here for the first time. The Gly_{10} linkers seem to affect the properties of the resulting artificial proteins, cell division, magnetosome production and protein expression. Therefore, seamless cloning[34] of the highly repetitive sequences is essential for spider silk proteins and their properties, even if expressed in a complex system like *M. gryphiswaldense*.

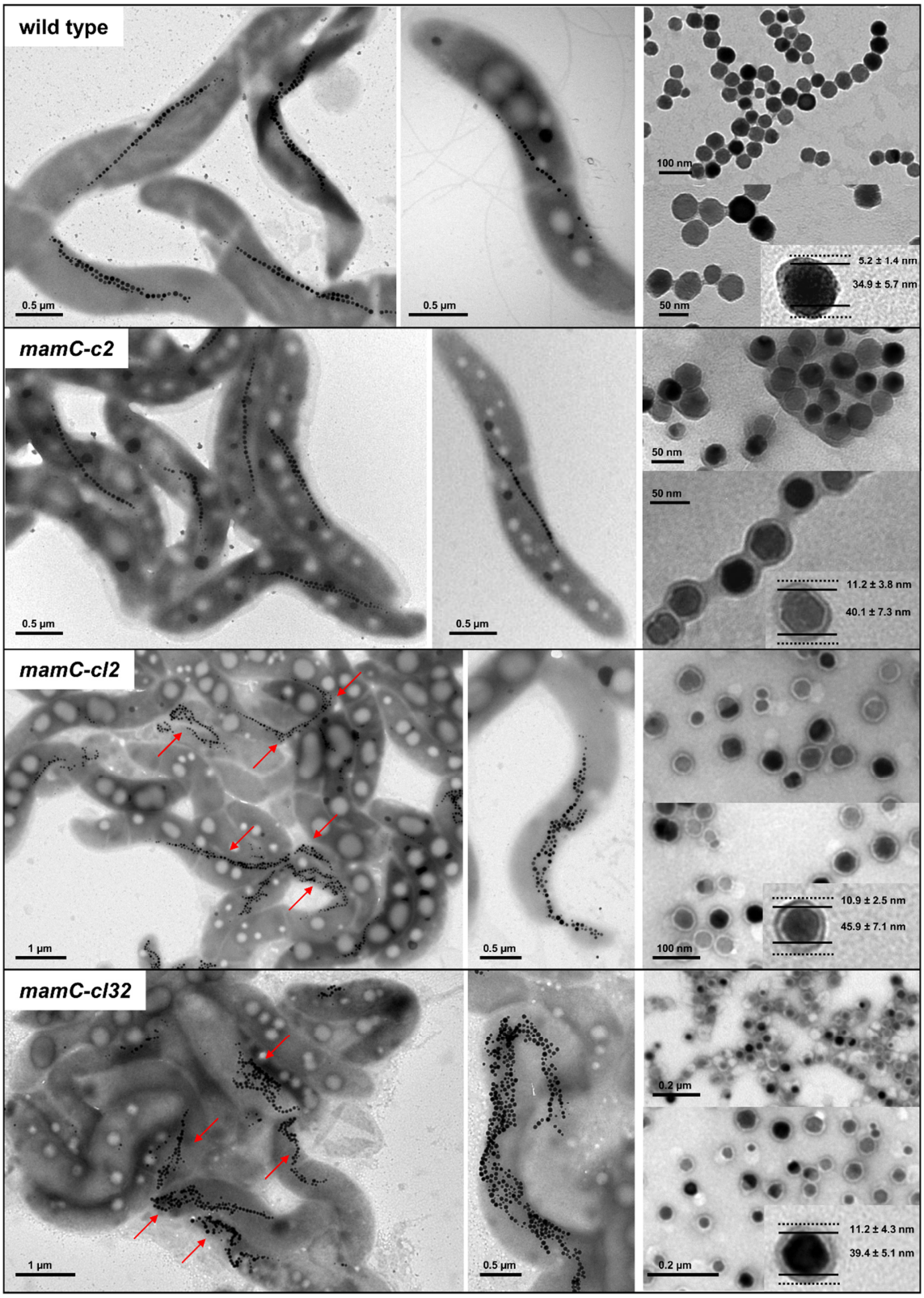
wild type
0.5 µm
0.5 µm
100 nm
5.2 ± 1.4 nm
34.9 ± 5.7 nm
50 nm
mamC-c2
0.5 µm
0.5 µm
50 nm
50 nm
11.2 ± 3.8 nm
40.1 ± 7.3 nm
mamC-cl2
1 µm
0.5 µm
10.9 ± 2.5 nm
45.9 ± 7.1 nm
100 nm
mamC-cl32
1 µm
0.5 µm
0.2 µm
11.2 ± 4.3 nm
39.4 ± 5.1 nm
0.2 µm

Figure 2. Transmission electron micrographs of cells and isolated, negatively stained particles from *M. gryphiswaldense* strains *mamC-c2*, *mamC-cl2*, *mamC-cl32*, and from the wild type. The spider silk motif expressing strains *mamC-cl2* and *mamC-cl32* showed a magnetosome misdistribution with more than 50% of the cells containing 70-120 particles per cell (see also Figure S4 and Figure S5). Furthermore, high ratios of nearly particle-free cells were visible. Arrows indicate cells overproducing magnetosomes. In contrast, *mamC-c2* cells formed wild type-like particle amounts (about 32 particles per cell, arranged in one or two chains positioned ad midcell). For all particles displaying spider silk motifs, a capsule of up to 15 nm in thickness was visible.

Intrigued by the perturbed cell separation phenotype, we studied the *mamC-cl32* cell division sites by cryo-electron tomography, a powerful technique to investigate the subcellular ultrastructure in a near-native state. Cells of *mamC-cl32* tended to form minicell-like structures at the division sites, before becoming eventually separated. Parts of the magnetosome chains were frequently trapped in and traversing the minicells (Figure 3 A-D, Figure S6 and S7), and the separation of individual cells was impaired. Hydrophobic interactions of the silk peptides might largely contribute to the forces to maintain the magnetosomes together in addition to the magnetostatic forces. The sum of both factors the hydrophobic surface interaction and the magnetic forces may likely lead to impairment for the cell in splitting the magnetosome chain properly, in turn generating the cell division defect, where cells seem to be caught in cytokinesis or forming minicell bridges with magnetosome chains confined inside. Even with the aid of the dynamic MamK filaments contributing to pole-to-midcell motion of the magnetosome chain,[55] the magnetosome surface hydrophobic forces are such that the cells cannot separate properly the

magnetosome chain, and higher forces might be required to overcome the magnetic and other non-covalent interactions between particles. Furthermore, binding of MamJ to the MamK filament might be impaired by the silk peptides displayed on the magnetosome surface, and it can be assumed that MamJ is inaccessible due to the proteinaceous spider silk capsule.

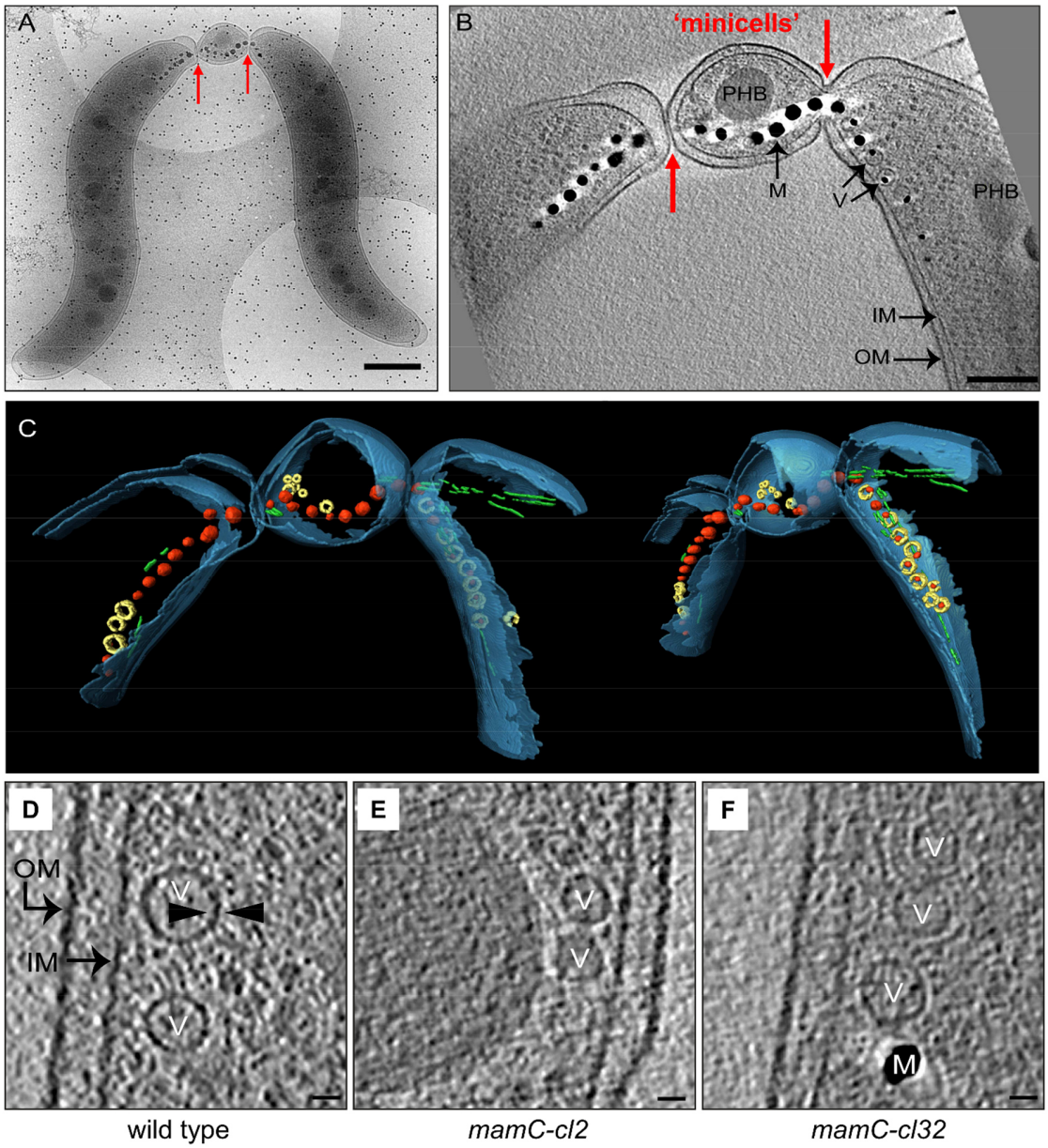

Figure 3. Cryo-electron tomography of selected strains. (A) Cryo-electron microscopy image of a *mamC-cl32* cell (n = 10) selected for tomography. Scale bar: 500 nm. (B) A 12.8 nm thick tomographic slice (average of 5 slices) displaying the division site of the cell shown in "A". Cells display impairment in cytokinesis generating bridges of minicells due to improper cell division. Division sites are indicated by red arrows. M: magnetite crystal, IM: inner membrane, OM: outer membrane, V: vesicle, PHB: polyhydroxybutyrate granule. Scale bar: 200 nm. (C) CET 3D rendering of the selected cell division site. Magnetite crystals: red, vesicles (magnetosome membrane): yellow, and MamK filament: green. The cellular envelope inner and outer membranes are depicted in blue. (D-F) Magnetosome vesicle visualization by cryo-electron tomograms. An 8.5 nm thick tomographic slice (average of 5 slices) of non-magnetic cells of (D) wild type (n = 9), (E) *mamC-cl2* (n = 8) and (F) *mamC-cl32* (n = 11) cultivated in low-iron medium for vesicle (magnetosome membrane) thickness comparison. V: vesicle (magnetosome membrane). M: magnetite crystal, OM: outer membrane, IM: inner membrane. Arrowheads indicate vesicle thickness. Scale bars: 20 nm.

Magnetosome expression of spider silk motifs generates a proteinaceous capsule

In SDS gels, MamC-C2 magnetosomes displayed an additional band of 20 kDa (Figure 4, red boxes), equivalent to the predicted molecular weight of the MamC-C2 hybrid protein. For *mamC-cl2* an expected band of 21 kDa (predicted molecular weight of the MamC-CL2 fusion) was absent; instead, an additional 150 kDa band could be detected. A protein of similar electrophoretic mobility was visible for *mamC-cl32*, corresponding to the predicted molecular weight of the MamC-CL32 fusion (156 kDa). In Western blots, for the wild type and MamC-mEGFP (=control construct) bands with the expected molecular weight were detected (wild type:

13 kDa, MamC-mEGFP: 39 kDa). For MamC-C2 particles, two bands with equal intensities but different electrophoretic mobilities (21 and 13 kDa) were obtained, corresponding to the expected molecular weight of the MamC-C2 hybrid protein and the unfused MamC (20 and 12 kDa, respectively) (Table 1). For MamC-CL32 two bands of high molecular weight (156 kDa and 144 kDa) with different intensities were detected (with the predominant band of 156 kDa corresponding to the predicted size of the MamC-CL32 fusion protein), while for the MamC-CL2 fusion the expected band of 21 kDa was absent, and high molecular weight bands of 154 kDa, 142 kDa and 83 kDa were detected instead (Table 1). This unexpected behavior might be partly caused by an altered binding behavior of SDS to the linker-modified proteins due to the Gly_{10} sequences.

Due to their highly hydrophobic character, it is not unlikely that the produced hybrid proteins (consisting of MamC and spider silk peptides) might interact with each other. However, the overall high abundance of magnetosome membrane proteins suggests an unusually crowded protein composition of the magnetosome membrane.[56] Therefore we assume that the tight packing with transmembrane domains of integral proteins would interfere with the formation of specific patches in the magnetosome membrane.

Proteomics analysis of polyacrylamide gel slices (Proteomics Service, Ludwig-Maximilians-University of Munich, Planegg-Martinsried, Germany) revealed a variety of cellular (enzyme) proteins and peptides (including MamC) present in the 150 and 140 kDa region of lanes “MamC-CL2” and “MamC-CL32”. However, distinct proteins with a molecular mass of 150 or 140 kDa could not be detected. An almost identical protein/peptide content pattern was obtained for gel slices from the “wild type” lane. Thus, in particular for the MamC-CL2 fusion these findings might argue for the presence of chimeric proteins on the particle surface, with increased

molecular masses that also involve other cellular proteins and peptides. Furthermore, for both CL fusions no unfused MamC was detectable, indicating that the latter might be incorporated in mixed assemblies with (chimeric) MamC-CL fusion proteins.

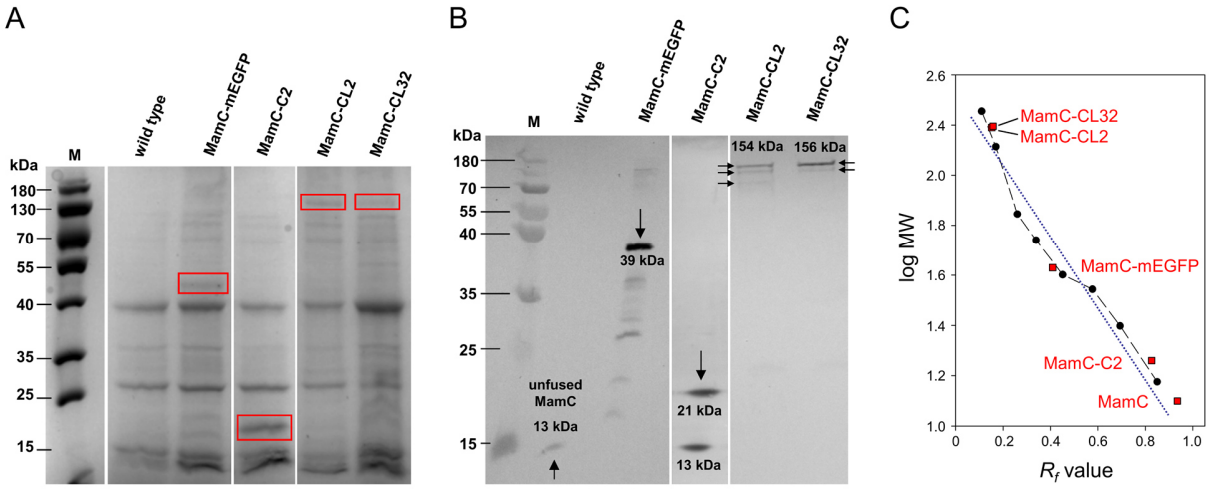

Figure 4. Magnetosome expression of spider silk motifs as translational fusions to MamC. (A) Solubilized protein fractions of isolated magnetosomes (32 µg Fe/lane) from the mutant strains *mamC-c2*, *mamC-cl2* and *mamC-cl32* of *M. gryphiswaldense* were subjected to denaturing PAGE. Fractions from wild type magnetosomes and from a Δ*mamC::mamC-megfp* transposon mutant (MamC-mEGFP)[18] were used as control. In the Coomassie-stained gel, similar patterns were obtained for all strains. However, depending on the proteins displayed on the magnetosome surface, additional bands (compared to the wild type) were detected (red boxes). For Δ*mamC::mamC-megfp*, an extra band of 39 kDa was visible, which corresponds to the MamC-mEGFP fusion. (B) Western blot analysis employing an IgG antibody directed against MamC was used for the detection of MamC fusion proteins. Degradation products potentially caused by the sample preparation were detected to only minor extents. M, protein molecular

weight marker. (C) Electrophoretic mobilities (and the corresponding R_f values) of the marker proteins were taken to draw a calibration curve and to estimate the molecular weight of MamC hybrid proteins.

Table 1. Molecular weight of MamC-C2, MamC-CL2 and MamC-CL32 hybrid proteins on the magnetosome surface. Denaturing PAGE with subsequent Western blotting (Figure 4) was used to estimate the molecular weight of the fusions according to their electrophoretic mobility. The obtained values are compared with the theoretical weights based on amino acid composition.

	MamC	**MamC-mEGFP**	**MamC-C2**	**MamC-CL2**	**MamC-CL32**
Predicted molecular weight (kDa)	12	39	20	21	160
Apparent molecular weight, estimated from Western blot (kDa)	13	39	21	154 / 142 / 83	156 / 144

TEM micrographs revealed that magnetosomes isolated from spider silk-expressing strains were surrounded by an organic capsule of low electron density (Figure 2, Table S4). For MamC-C2, MamC-CL2 and MamC-CL32, the thickness of this layer was about 11 nm, with overall particle diameters of 52.6 and 56.8 nm, respectively. The expression of silk motifs with 32 repetitive units (MamC-CL32) also resulted in a layer of 11 nm, and therefore in similar particle sizes. Thus, particle diameters were considerably increased compared to wild type magnetosomes (38.1 nm in diameter) or MamC-mEGFP particles (39.7 nm in diameter), which were used as an additional control because the latter display up to 200 mEGFP copies on the surface.[18] For spider

silk magnetosomes, neither the presence of Gly_{10} linkers nor the number of spider silk motifs did affect layer thickness and particle diameters. A possible explanation is that linker constructs may closely adhere (in a flat layer) to the magnetosome surface and by that the surface is blocked by a protein layer. Increased particle sizes were essentially confirmed by zetasizer measurements revealing diameters of up to 63.5 ± 5.8 nm (for strain *mamC-cl32*) (Table S4).

In contrast, cryo-electron tomography of iron-starved cells (mostly devoid of magnetite crystals) of the wild type, *mamC-cl2* and *mamC-cl32* strains (C_{mag} = 0.42, 0.2 or 0.2, respectively) revealed no apparent differences in vesicle features *in situ* (i.e., same electron density, shape, diameter), with membrane thickness determined as 6.1 ± 0.1 (SEM) and 6.0 ± 0.1 (SEM) for the wild type and *mamC-cl32*, respectively (Figure 3 and Figure S8). This can be explained as that the protein layers residing on the magnetosome membrane are not sufficiently electron-dense to be detected.

Effects of the displayed silk peptides on magnetosome biosynthesis by potential misorganization of magnetosome membrane proteins (like e.g. MamA) and/or impaired interactions with other (magnetosome) proteins are rather unlikely since it has been shown that even the magnetosome expression of large enzyme arrays (with up to 90% coverage of the particle surface) has no influence on magnetosome biomineralization.[25]

Fourier transform infrared spectroscopy (FTIR) was used to obtain further information on the organic layer on the magnetosome surface (Figure S9). Of particular interest were bands in the C=O stretch vibration regime (1780 - 1585 cm^{-1}), which contain information on the phospholipid portion (esters, acids: ~ 1750 - 1710 cm^{-1}) and protein portion (amide I: ~ 1690 - 1600 cm^{-1}). Protein to phospholipid ratios calculated from phospholipid and amide I band maxima

($A_{norm.}$(amide I)/$A_{norm.}$(phospholipids)) were 3.54 for wild type and 3.41 for MamC-mEGFP particles, indicating the presence of proteins on the surface as expected. Similar values were obtained for particles of MamC-CL2 and MamC-CL32 magnetosomes, with ratios of 3.77 and 3.02, respectively. By contrast, for magnetosome preparations in which the native enveloping membrane was partially lost (for instance during preparation), we observed reduced protein to phospholipid ratios (MamC-CL2: 0.11, MamC-CL32: 0.10 and 0.41; Figure S9) revealing low protein amounts on the magnetosome surface. Therefore, ATR-FTIR can be used as qualitative method for examination of protein expression and the proper preservation of the magnetosomes membrane. For MamC-C2, a protein-to-phospholipid ratio of 6.19 was measured, indicating a high C2-expression on the magnetosome surface in agreement with the detection of this construct by Western blot and the improved compatibility with the expression system (indicated by reduced effects on cell growth and division). The amide I band is a superposition of C=O stretching vibrations of the protein backbone (peptide bond) which are influenced in their vibrational energy depending on the chemical environment. Secondary structures were assigned to specific wavenumber regions of the amide I band based on secondary structure assignment of recombinant spider silk protein eADF4(C16).[57] All samples (wild type, MamC-mEGFP, MamC-C2, MamC-CL2 and MamC-CL32) showed a maximum in the α-helical regime (1656 - 1653 cm^{-1}). For MamC-mEGFP and in particular for MamC-CL2 / 32 constructs, an increase of the shoulder in the region from 1640 - 1625 cm^{-1} was visible (Figure S9). These spectra therefore indicate differences in secondary structure elements (for instance, β-sheet content). mEGFP forms β-barrel-like structures,[58,59] and compared to wild type magnetosomes MamC-mEGFP particles exhibited a slight increase of the shoulder in the β-sheet regime. In contrast, for the MamC-C2 construct spectra were comparable to those of wild type magnetosomes (no shoulder

in the region from 1640 - 1625 cm^{-1}) indicating the absence of β-sheets, which is consistent with the assumption that MamC-C2 only forms a minor β-sheet portion due to the small size of the fusion and the low number of C-module repeats.

Physico-chemical characteristics of MamC-C2, MamC-CL2 and MamC-CL32 magnetosomes

Next, we investigated the sedimentation behavior of MamC-C2, MamC-CL2 and MamC-CL32 magnetosomes (Figure S10). For wild type magnetosomes linear sedimentation profiles were observed, reflected by absorption ratios that significantly decreased with time. MamC-C2 and MamC-CL2 / 32 particles also showed linear sedimentation patterns; however, absorption ratios only slightly decreased, and MamC-CL32 particle suspensions remained nearly stable (i.e., did not sediment) for more than 200 min. Although MamC-C2 and MamC-CL2 magnetosomes exhibited a higher tendency to settle down, absorption ratios were still significantly higher compared to that of wild type particles (up to 30% for MamC-C2). Furthermore, the zeta potential (ZP) of silk motif-expressing particles shifted to more negative values (wild type: -34.8 ± 5.3 mV; MamC-C2: -37.2 ± 3.9 mV; MamC-CL2: -37.2 ± 4.0 mV; MamC-CL32: -45.2 ± 4.5 mV). An ANOVA test confirmed that the overall difference between the means was significant ($P < 0.001$). The observed shift in the ZP values might be attributed to negatively charged amino acid residues (e.g. glutamate residues) of the silk motifs or (in case of MamC-CL2/32 linker constructs) additional unspecifically bound protein compounds. These residues would add an additional charge to the particle surface when exposed to the solvent. The theoretical pI values of C2, CL2 and CL32 were calculated[60] to be 3.79, 3.79 and 2.87 and indicate negatively charged

protein species at a given pH of 7.2. Therefore, decreased sedimentation rates might be explained by electrostatic repulsion, and increased spacing between the magnetite cores (caused by the silk capsule) might lead to reduced magnetic interactions. Thus, the presence of the spider silk capsule reduced sedimentation and increased colloidal stability of the suspensions.

MamC-C2 magnetosomes act as seeds for spider silk fibril growth

Although nucleation is a thermodynamically disfavored process and the rate limiting step[61] of eADF4(C16) fibril formation, it can be surpassed upon the addition of preformed seeds, which enable docking of monomers and thus, trigger fibril formation.[36,62] *Humenik et al.* showed that silk particles can interact with monomeric eADF4(C16),[62] resulting in fibril growth from their surface. In order to analyze potential interactions of MamC-C2 or wild type magnetosomes with material surfaces made of eADF4(C16), QCM-D measurements were performed. MamC-C2 magnetosomes exhibited adsorption rates on eADF4(C16) films that were increased compared to that of wild type particles. Furthermore, for MamC-C2 particles a more linear adsorption behavior was observed, and one can assume that MamC-C2 magnetosomes interacted with eADF4(C16) by intermolecular interactions. Due to shown interaction of MamC-C2 with eADF4(C16), we further investigated whether MamC-C2 magnetosomes enabled docking of soluble eADF4(C16) on the magnetosome surface and triggered fibril formation. Therefore, MamC-C2 magnetosomes were incubated with freshly dialyzed eADF4(C16). TEM micrographs revealed the formation of fibrillar structures arising from single magnetosomes or magnetosome chains at similar rates (Figure 5B and Figure S11). In contrast, on wild type particles no indications for directed fibril growth from the particle surfaces were detectable (Figure 5A).

These findings suggest that magnetosome surface exposed spider silk peptides can function as fibrillization seeds, and thus can trigger fibril growth by recruiting eADF4(C16) out of solution (Figure 5C).

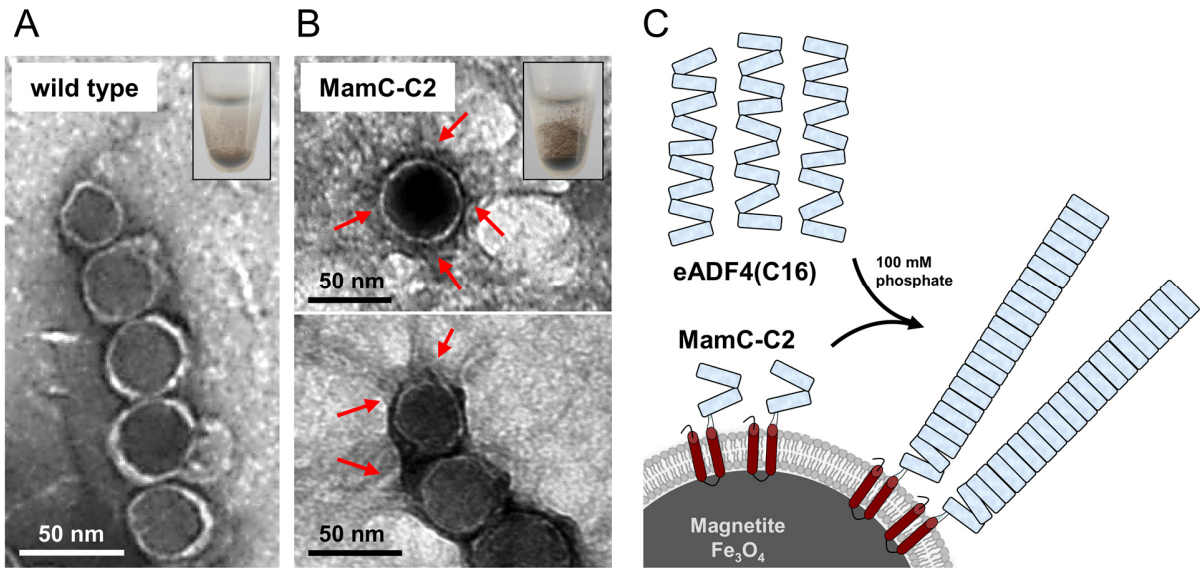

Figure 5. Assembly of nanofibrils in the presence of MamC-C2 magnetosomes. TEM micrographs of isolated wild type particles (A) or MamC-C2 magnetosomes (B) that were incubated with 20 µM freshly dialyzed eADF4(C16) monomers in potassium phosphate buffer. For wild type magnetosomes no indications for directed fibril growth from the particle surfaces were detectable, whereas for MamC-C2 magnetosomes fibril-like structures were visible at the particle surface (indicated by arrows), suggesting C2 triggered docking of further eADF4(16) monomers and fibril formation on the magnetosome surface (C) as it has been observed for silk particles by Humenik and co-workers.[62] Insets: During incubation with eADF4(C16) monomers, in the presence of MamC-C2 magnetosomes fibrous, network-like structures were visible in the reaction tube. These structures were not observed for wild type magnetosomes.

Conclusions

We for the first time demonstrated that recombinant spider silk peptides (MamC-C2) can be expressed in a magnetotactic bacterium. The need of a seamless cloning strategy[34] preserving the highly repetitive hydrophobic character of silk proteins[52,54] was experimentally confirmed as disturbances in the sequence, like the introduced Gly_{10} linkers (MamC-CL2, MamC-CL32), affect the silk properties and even lead to affection of cell division, magnetosome production and protein expression. In contrast, magnetosome display of a (linker-less) C2 silk motif as hybrid protein fused to an abundant magnetosome membrane anchor in *M. gryphiswaldense* caused the formation of a proteinaceous coat with exposed spider silk features (specific interaction with materials made of eADF4(C16) as well as seeding/nucleating fibrillar growth from the surface) and thus provides a promising route for encapsulation and functionalization of bacterial nanoparticles. Since spider silk is non-immunogenic,[63] in future applications such building blocks might improve the biocompatibility of bacterial magnetosomes and mask immunogenic compounds displayed on the particle surface. Our strategy demonstrates that the surface properties of magnetic nanoparticles can be further tuned, as particle agglomeration was reduced and the colloidal stability increased. Magnetosome expression of spider silk-inspired peptides could be used in future approaches to generate multifunctional nanoparticles combining those features with further functionalities, such as catalytic activities, and to produce magnetic silk composites that can be oriented and manipulated by an external magnetic field.[64] In summary, our results provide a route towards the generation of fully genetically encoded, functionalized hybrid composites that might be useful as novel biomaterials with enhanced properties in biotechnological and biomedical applications.

ASSOCIATED CONTENT

Supporting Information

The Supporting Information is available free of charge on the ACS Publications website.

Supporting Information (PDF):

Schematics illustrating the generation of *mamC-cl2* and *mamC-cl32* constructs; charts / tables showing magnetosome distributions, cellular iron contents, particle sizes and layer thicknesses of spider silk-decorated magnetosomes; cryo-electron tomography data; normalized FTIR absorption spectra of magnetosome samples showing bands in the C=O stretch vibration regime; normalized absorption values reflecting the sedimentation behavior of spider silk coated magnetosomes; TEM micrographs illustrating the assembly of nanofibrils in the presence of MamC-C2 magnetosomes.

Supplemental Movie M1:

Cryo-electron tomography and three dimensional rendering of a *mamC-cl32* cell division site. View through the z-stack tomogram of the division site of *mamC-cl32* connected cells by a minicell bridge at a 27,500× magnification. Cellular envelope (blue), vesicles (yellow) and magnetite (red) associated to the MamK filament structure (green). Movie M1 is related to Figure 3.

AUTHOR INFORMATION

Corresponding Author

* Prof. D. Schüler

E-mail: Dirk.Schueler@uni-bayreuth.de

Department Microbiology, University of Bayreuth, Universitätsstraße 30, D-95447 Bayreuth, Germany

Tel.: +49-921-552728

Fax: +49-921-552727

Author Contributions

FM, DS and TS designed the study. FM generated spider silk-expressing strains and performed cultivation experiments, magnetosome isolation, sedimentation assays, electron microscopy and zetasizer measurements; FM analysed and interpreted the obtained data. CBB designed, performed and optimized QCM-D and ATR-FTIR experiments and analysed the data. MT-N performed cryo-electron tomography experiments; MT-N and JMP analysed the data. MT-N performed 3D rendering of tomographed cells and the corresponding movie. HMH carried out fibrillization experiments. DSM prepared samples for and performed gel electrophoreses and Western blotting. FM took the lead in writing the manuscript. All authors provided critical feedback and helped shape the research, analysis and manuscript.

Funding Sources

Deutsche Forschungsgemeinschaft (grants DFG SCHU 1080/15-3 and SCHU 1080/9-2 to D.S., and SCHE 603/15-2 to T.S.); European Research Council (ERC AdG Syntomagx to D.S.)

Notes

The authors declare no competing financial interest.

ACKNOWLEDGMENT

We are grateful to S. Borg for providing several expression plasmids, M. Schlotter (University of Bayreuth) for expert technical assistance, and Günter Pfeifer, Rubén Fernández-Busnadiego and Tillman Schäfer (MPI of Biochemistry) for constant support with cryo-electron tomography. This project was funded by the Deutsche Forschungsgemeinschaft (grants DFG SCHU 1080/15-3 and SCHU 1080/9-2 to D.S., SCHE 603/15-2 to T.S.) and the European Research Council (ERC AdG Syntomagx to D.S.).

REFERENCES

(1) Komeili, A. Molecular Mechanisms of Compartmentalization and Biomineralization in Magnetotactic Bacteria. *FEMS Microbiol. Rev.* **2012**, *36*, 232-255.

(2) Uebe, R.; Schüler, D. Magnetosome Biogenesis in Magnetotactic Bacteria. *Nat. Rev. Microbiol.* **2016**, *14*, 621-637.

(3) Jogler, C.; Schüler, D. Genomics, Genetics, and Cell Biology of Magnetosome Formation. *Annu. Rev. Microbiol.* **2009**, *63*, 501-521.

(4) Staniland, S. S.; Ward, B.; Harrison, A.; van der Laan, G.; Telling, N. Rapid Magnetosome Formation Shown by Real-Time X-Ray Magnetic Circular Dichroism. *Proc. Natl. Acad. Sci. U.S.A.* **2007**, *104*, 19524-19528.

(5) Staniland, S. S.; Rawlings, A. E. Crystallizing the Function of the Magnetosome Membrane Mineralization Protein Mms6. *Biochem. Soc. Trans.* **2016**, *44*, 883-890.

(6) Pollithy, A.; Romer, T.; Lang, C.; Müller, F. D.; Helma, J.; Leonhardt, H.; Rothbauer, U.; Schüler, D. Magnetosome Expression of Functional Camelid Antibody Fragments (Nanobodies) in Magnetospirillum gryphiswaldense. *Appl. Environ. Microbiol.* **2011**, *77*, 6165-6171.

(7) Tanaka, T.; Takeda, H.; Ueki, F.; Obata, K.; Tajima, H.; Takeyama, H.; Goda, Y.; Fujimoto, S.; Matsunaga, T. Rapid and Sensitive Detection of 17Beta-Estradiol in Environmental Water Using Automated Immunoassay System with Bacterial Magnetic Particles. *J. Biotechnol.* **2004**, *108*, 153-159.

(8) Lang, C.; Schüler, D.; Faivre, D. Synthesis of Magnetite Nanoparticles for Bio- and Nanotechnology: Genetic Engineering and Biomimetics of Bacterial Magnetosomes. *Macromol. Biosci.* **2007**, *7*, 144-151.

(9) Hergt, R.; Dutz, S.; Röder, M. Effects of Size Distribution on Hysteresis Losses of Magnetic Nanoparticles for Hyperthermia. *J. Phys. Condens. Matter* **2008**, *20*, 385214.

(10) Alphandéry, E.; Guyot, F.; Chebbi, I. Preparation of Chains of Magnetosomes, Isolated from Magnetospirillum magneticum Strain AMB-1 Magnetotactic Bacteria, Yielding

Efficient Treatment of Tumors Using Magnetic Hyperthermia. *Int. J. Pharm.* **2012**, *434*, 444-452.

(11) Taukulis, R.; Widdrat, M.; Kumari, M.; Heinke, D.; Rumpler, M.; Tompa, É.; Uebe, R.; Kraupner, A.; Cebers, A.; Schüler, D.; Pósfai, M.; Hirt, A. M.; Faivre, D. Magnetic Iron Oxide Nanoparticles as MRI Contrast Agents - a Comprehensive Physical and Theoretical Study. *Magnetohydrodynamics* **2015**, *51*, 721-747.

(12) Herborn, C. U.; Papanikolaou, N.; Reszka, R.; Grünberg, K.; Schüler, D.; Debatin, J. F. Magnetosomen als biologisches Modell der Eisenbindung: Messung der Relaxivität in der MRT. *Fortschr. Röntgenstr.* **2003**, *175*, 830-834.

(13) Kraupner, A.; Eberbeck, D.; Heinke, D.; Uebe, R.; Schüler, D.; Briel, A. Bacterial Magnetosomes - Nature's Powerful Contribution to MPI Tracer Research. *Nanoscale* **2017**, *9*, 5788-5793.

(14) Grünberg, K.; Wawer, C.; Tebo, B. M.; Schüler, D. A Large Gene Cluster Encoding Several Magnetosome Proteins is Conserved in Different Species of Magnetotactic Bacteria. *Appl. Environ. Microbiol.* **2001**, *67*, 4573-4582.

(15) Scheffel, A.; Gärdes, A.; Grünberg, K.; Wanner, G.; Schüler, D. The Major Magnetosome Proteins MamGFDC are not Essential for Magnetite Biomineralization in Magnetospirillum gryphiswaldense but Regulate the Size of Magnetosome Crystals. *J. Bacteriol.* **2008**, *190*, 377-386.

(16) Grünberg, K.; Müller, E. C.; Otto, A.; Reszka, R.; Linder, D.; Kube, M.; Reinhardt, R.; Schüler D. Biochemical and Proteomic Analysis of the Magnetosome Membrane in Magnetospirillum gryphiswaldense. *Appl. Environ. Microbiol.* **2004**, *70*, 1040-1050.

(17) Lang, C.; Schüler, D. Expression of Green Fluorescent Protein Fused to Magnetosome Proteins in Microaerophilic Magnetotactic Bacteria. *Appl. Environ. Microbiol.* **2008**, *74*, 4944-4953.

(18) Borg, S.; Hofmann, J.; Pollithy, A.; Lang, C.; Schüler, D. New Vectors for Chromosomal Integration Enable High-Level Constitutive or Inducible Magnetosome Expression of Fusion Proteins in Magnetospirillum gryphiswaldense. *Appl. Environ. Microbiol.* **2014**, *80*, 2609-2616.

(19) Nudelman, H.; Zarivach, R. Structure Prediction of Magnetosome-Associated Proteins. *Front. Microbiol.* **2014**, *5*, 9.

(20) Borg, S.; Popp, F.; Hofmann, J.; Leonhardt, H.; Rothbauer, U.; Schüler, D. An Intracellular Nanotrap Redirects Proteins and Organelles in Live Bacteria. *mBio* **2015**, *6*, e02117-14.

(21) Yoshino, T.; Matsunaga, T. Efficient and Stable Display of Functional Proteins on Bacterial Magnetic Particles Using Mms13 as a Novel Anchor Molecule. *Appl. Environ. Microbiol.* **2006**, *72*, 465-471.

(22) Ohuchi, S.; Schüler, D. In Vivo Display of a Multisubunit Enzyme Complex on Biogenic Magnetic Nanoparticles. *Appl. Environ. Microbiol.* **2009**, *75*, 7734-7738.

(23) Ginet, N.; Pardoux, R.; Adryanczyk, G.; Garcia, D.; Brutesco, C.; Pignol, D. Single-Step Production of a Recyclable Nanobiocatalyst for Organophosphate Pesticides Biodegradation Using Functionalized Bacterial Magnetosomes. *PLoS One* **2011**, *6*, e21442.

(24) Kolinko, I.; Jogler, C.; Katzmann, E.; Schüler, D. Frequent Mutations within the Genomic Magnetosome Island of Magnetospirillum gryphiswaldense are Mediated by RecA. *J. Bacteriol.* **2011**, *193*, 5328-5334.

(25) Mickoleit, F.; Schüler, D. Generation of Multifunctional Magnetic Nanoparticles with Amplified Catalytic Activities by Genetic Expression of Enzyme Arrays on Bacterial Magnetosomes. *Adv. Biosyst.* **2017**, 1700109.

(26) Sabourin, M.; Tuzon, C.; Fisher, T.; Zakian, V. A Flexible Protein Linker Improves the Function of Epitope-Tagged Proteins in Saccharomyces cerevisiae. *Yeast* **2007**, *24*, 39-45.

(27) Borg, S.; Rothenstein, D.; Bill, J.; Schüler, D. Generation of Multishell Magnetic Hybrid Nanoparticles by Encapsulation of Genetically Engineered and Fluorescent Bacterial Magnetosomes with ZnO and SiO2. *SMALL* **2015**, *11*, 4209-4217.

(28) Vollrath, F. Strength and Structure of Spiders' Silks. *Rev. Mol. Biotechnol.* **2000**, *74*, 67-83.

(29) Bini, E.; Knight, D. P.; Kaplan, D. L. Mapping Domain Structures in Silks from Insects and Spiders Related to Protein Assembly. *J. Mol. Biol.* **2004**, *335*, 27-40.

(30) Leal-Egaña, A.; Scheibel, T. Silk-Based Materials for Biomedical Applications. *Biotechnol. Appl. Biochem.* **2010**, *55*, 155-167.

(31) Fahnestock, S. In W. E. I. DuPont (Ed.), Novel, recombinantly produced spider silk analogs. USA 1994, int. patent number: WO 94/29450.

(32) Heidebrecht, A.; Scheibel, T. Recombinant Production of Spider Silk Proteins. *Adv. Appl. Microbiol.* **2013**, *82*, 115-153.

(33) Widmaier, D. M.; Tullman-Ercek, D.; Mirsky, E. A.; Hill, R.; Govindarajan, S.; Minshull, J.; Voigt, C. A. Engineering the Salmonella Type III Secretion System to Export Spider Silk Monomers. *Mol. Syst. Biol.* **2009**, DOI: 10.1038/msb.2009.62

(34) Huemmerich, D.; Helsen, C. W.; Quedzuweit, S.; Oschmann, J.; Rudolph, R.; Scheibel, T. Primary Structure Elements of Spider Dragline Silks and their Contribution to Protein Solubility. *Biochemistry* **2004**, *43*, 13604-13612.

(35) Rammensee, S.; Slotta, U.; Scheibel, T.; Bausch, A. R. Assembly Mechanism of Recombinant Spider Silk Proteins. *Proc. Natl. Acad. Sci. U.S.A.* **2008**, *105*, 6590-6595.

(36) Humenik, M.; Magdeburg, M.; Scheibel, T. Influence of Repeat Numbers on Self-Assembly Rates of Repetitive Recombinant Spider Silk Proteins. *J. Struct. Biol.* **2014**, *186*, 431-437.

(37) Exler, J. H.; Hummerich, D.; Scheibel, T. The Amphiphilic Properties of Spider Silks are Important for Spinning. *Angew. Chem. Int. Ed.* **2007**, *46*, 3559-3562.

(38) Hagn, F.; Thamm, C.; Scheibel, T.; Kessler, H. pH-Dependent Dimerization and Salt-Dependent Stabilization of the N-Terminal Domain of Spider Dragline Silk-Implications for Fiber Formation. *Angew. Chem. Int. Ed.* **2011**, *50*, 310-313.

(39) Heyen, U.; Schüler, D. Growth and Magnetosome Formation by Microaerophilic Magnetospirillum Strains in an Oxygen-Controlled Fermentor. *Appl. Microbiol. Biotechnol.* **2003**, *61*, 536-544.

(40) Sambrook, J.; Russell, D. Molecular Cloning: a Laboratory Manual, 3rd ed; *Cold Spring Harbor Laboratory Press*: New York, NY, 2001; p 1-44.

(41) Schüler, D.; Rainer, U.; Bäuerlein, E. A Simple Light Scattering Method to Assay Magnetism in Magnetospirillum gryphiswaldense. *FEMS Microbiol. Lett.* **1995**, *132*, 139-145.

(42) Phenrat, T.; Saleh, N.; Sirk, K.; Tilton, R. D.; Lowry, G. Aggregation and Sedimentation of Aqueous Nanoscale Zerovalent Iron Dispersions. *Environ. Sci. Technol.* **2007**, *41*, 284-290.

(43) Tiraferri, A.; Chen, K. L.; Sethi, R.; Elimelech, M. Reduced Aggregation and Sedimentation of Zero-Valent Iron Nanoparticles in the Presence of Guar Gum. *J. Colloid Interface Sci.* **2008**, *324*, 71-79.

(44) Laemmli, U. K. Cleavage of Structural Proteins During the Assembly of the Head of Bacteriophage T4. *Nature* **1970**, *227*, 680-685.

(45) Fling, S. P.; Gregerson, D. S. Peptide and Protein Molecular Weight Determination by Electrophoresis Using a High-Molarity Tris Buffer System Without Urea. *Anal. Biochem.* **1986**, *155*, 83-88.

(46) Mastronarde, D. N. Automated Electron Microscope Tomography Using Robust Prediction of Specimen Movements. *J. Struct. Biol.* **2005**, *152*, 36-51.

(47) Kremer, J. R.; Mastronarde, D. N.; McIntosh, J. R. Computer Visualization of Three-Dimensional Image Data Using IMOD. *J. Struct. Biol.* **1996**, *116*, 71-76.

(48) Martinez-Sanchez, A.; Garcia, I.; Asano, S.; Lucic, V.; Fernandez, J. J. Robust Membrane Detection Based on Tensor Voting for Electron Tomography. *J. Struct. Biol.* **2014**, *186*, 49-61.

(49) Sauerbrey, G. Use of a Quartz Vibrator from Weighing Thin Films on a Microbalance. *Z. Phys.* **1959**, *155*, 206-222.

(50) Liu, G.; Zhang, G. Chapter 1: Basic Principles of QCM-D. (In) S. K. Sharma (ed): *QCM-D Studies on Polymer Behavior at Interfaces*; SpringerBriefs in Molecular Science, Springer Heidelberg New York Dordrecht London, 2013; pp 1-8.

(51) Xia, X. X.; Qian, Z. G.; Ki, C. S.; Park, Y. H.; Kaplan, D. L.; Lee, S. Y. Native-Sized Recombinant Spider Silk Protein Produced in Metabolically Engineered Escherichia coli Results in a Strong Fiber. *Proc. Natl. Acad. Sci. U.S.A.* **2010**, *107*, 14059-14063.

(52) Zbilut, J. P.; Scheibel, T.; Huemmerich, D.; Webber, C. L. Jr.; Colafranceschi, M.; Giuliani, A. Statistical Approaches for Investigating Silk Properties. *Appl. Phys. A* **2006**, *82*, 243-251.

(53) Lohße, A.; Kolinko, I.; Raschdorf, O.; Uebe, R.; Borg, S.; Brachmann, A.; Plitzko, J. M.; Müller, R.; Zhang, Y.; Schüler, D. Overproduction of Magnetosomes by Genomic Amplification of Biosynthesis-Related Gene Clusters in a Magnetotactic Bacterium. *Appl. Environ. Microbiol.* **2016**, *82*, 3032-3041.

(54) Zbilut, J. P.; Scheibel, T.; Huemmerich, D.; Webber, C. L. Jr.; Colafranceschi, M.; Giuliani, A. Spatial Stochastic Resonance in Protein Hydrophobicity. *Phys. Lett. A* **2005**, *346*, 33-41.

(55) Toro-Nahuelpan, M.; Müller, F. D.; Klumpp, S.; Plitzko, J. M.; Bramkamp, M.; Schüler, D. Segregation of Prokaryotic Magnetosomes Organelles is Driven by Treadmilling of a Dynamic Actin-Like MamK Filament. *BMC Biol.* **2016**, *14*, 88.

(56) Raschdorf, O.; Bonn, F.; Zeytuni, N.; Zarivach, R.; Becher, D.; Schüler, D. A Quantitative Assessment of the Membrane-Integral Sub-Proteome of a Bacterial Magnetic Organelle. *J. Prot*. **2018**, *172*, 89-99.

(57) Slotta, U.; Tammer, M.; Kremer, F.; Koelsch, P.; Scheibel, T. Structural Analysis of Spider Silk Films. *Supramol. Chem.* **2006**, *18*, 465-471.

(58) Ormö, M.; Cubitt, A. B.; Kallio, K.; Gross, L. A.; Tsien, R. Y.; Remington, S. J. Crystal Structure of the Aequorea victoria Green Fluorescent Protein. *Science* **1996**, *273*, 1392-1395.

(59) Yang, F.; Moss, L. G.; Phillips, G. N. Jr. The Molecular Structure of Green Fluorescent Protein. *Nature Biotech.* **1996**, *14*, 1246-1251.

(60) Gasteiger, E.; Hoogland, C.; Gattiker, A.; Duvaud, S.; Wilkins, M. R.; Appel, R. D.; Bairoch, A. Protein Identification and Analysis Tools on the ExPASy Server; (In) John M. Walker (ed): *The Proteomics Protocols Handbook*; Humana Press, 2005; pp 571-607.

(61) Jarrett, J. T.; Lansbury, P. T. Jr. Seeding "One-Dimensional Crystallization" of Amyloid: a Pathogenic Mechanism in Alzheimer's Disease and Scrapie? *Cell* **1993**, *73*, 1055-1058.

(62) Humenik, M.; Smith, A. M.; Arndt, S.; Scheibel, T. Ion and Seed Dependent Fibril Assembly of a Spidroin Core Domain. *J. Struct. Biol.* **2015**, *191*, 130-138.

(63) Spiess, K.; Lammel, A.; Scheibel, T. Recombinant Spider Silk Proteins for Applications in Biomaterials. *Biosci.* **2010**, *10*, 998-1007.

(64) Mayes, E.L.; Vollrath, F.; Mann, S. Fabrication of Magnetic Spider Silk and Other Silk-Fiber Composites Using Inorganic Nanoparticles. *Adv. Mater.* **1998**, *10*, 801-805.

ToC Figure

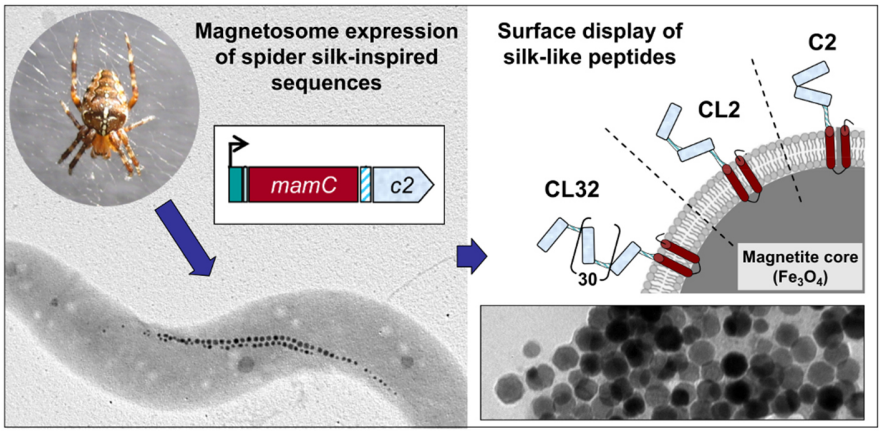
Magnetosome expression of spider silk-inspired sequences
mamC
c2
Surface display of silk-like peptides
C2
CL2
CL32
30
Magnetite core (Fe_3O_4)